

Single domain magnetic helicity and triangular chirality in structurally enantiopure $\text{Ba}_3\text{NbFe}_3\text{Si}_2\text{O}_{14}$

K. Marty,¹ V. Simonet,¹ E. Ressouche,² R. Ballou,¹ P. Lejay,¹ and P. Bordet¹

¹*Institut Néel, CNRS & Université Joseph Fourier, BP166, 38042 Grenoble, France*

²*Institut Nanosciences et Cryogenie, SPSMS/MDN, CEA-Grenoble, 38054 Grenoble, France*

(Dated: December 14, 2008)

A novel doubly chiral magnetic order is found out in the structurally chiral langasite compound $\text{Ba}_3\text{NbFe}_3\text{Si}_2\text{O}_{14}$. The magnetic moments are distributed over planar frustrated triangular lattices of triangle units. On each of these they form the same triangular configuration. This ferrochiral arrangement is helically modulated from plane to plane. Unpolarized neutron scattering on a single crystal associated with spherical neutron polarimetry proved that a single triangular chirality together with a single helicity is stabilized in an enantiopure crystal. A mean-field analysis allows to discern the relevance on this selection of a twist in the plane to plane supersuperexchange paths.

PACS numbers: 75.25.+z, 77.84.-s, 75.10.Hk

Chirality is the geometric property of an object according to which this exists in two distinct enantiomorphic states that are images of each other by space inversion but cannot be brought into coincidence by direct Euclidian isometry, namely spatial proper rotation and translation, eventually combined with time reversal [1]. An example in magnetism is the left or right handedness associated with the helical order of magnetic moments. Such an order may emerge from spontaneous symmetry breaking in systems with competing exchange interactions [2, 3] or from the instability of simple magnetic orders with respect to Dzyaloshinskii-Moriya anti-symmetric exchange interactions [4, 5, 6, 7]. The parity symmetry is globally restored in the case of a centrosymmetric structure by the presence in the same crystal of equally populated domains of opposite chirality states, which can be unbalanced only through axial-polar, magnetoelastic or magnetoelectric, field couplings [8, 9]. A single domain should be selected in non-centrosymmetric compounds where the parity symmetry is explicitly broken [10, 11]. So far this was reported only in the intermetallic compound MnSi [12]. Another example of magnetic chirality is the clockwise or anticlockwise asymmetry associated with the triangular configuration of frustrated magnetic moments on a triangular plaquette with antiferromagnetic interactions. Actual magnets exhibiting this triangular chirality [13], eventually coexisting with the helical chirality [14], are scarce and none was found in a single domain chiral state. With edge-sharing plaquettes the choice of a chirality state on one triangle fixes to opposite the chirality state on the adjacent triangles [15]. No such constraint exists in the kagomé lattice of corner-sharing triangles. Anti-symmetric exchange interactions, allowed in this case, can select a uniform distribution of a chirality state [16], but this is altered by low energy defects [17], bringing about alternative chirality textures. We hereafter report on an attractive material, $\text{Ba}_3\text{NbFe}_3\text{Si}_2\text{O}_{14}$, where the two magnetic chiralities coexist, are single domain, and are fixed with respect to the

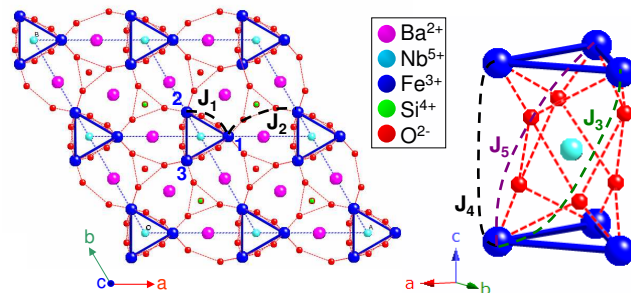


FIG. 1: (Color online) $\text{Ba}_3\text{NbFe}_3\text{Si}_2\text{O}_{14}$ crystal structure as projected in the (a, b) plane and viewed as stacked along the trigonal c -axis. The Fe^{3+} triangles are shown with solid lines. The super and supersuperexchange paths are depicted with short-dashed lines. The J_1 to J_5 exchange links are schematized by long-dashed lines.

structural chirality.

$\text{Ba}_3\text{NbFe}_3\text{Si}_2\text{O}_{14}$ crystallizes in the $P321$ non-centrosymmetric trigonal space group and is isostructural to $\text{La}_3\text{Ga}_5\text{SiO}_{14}$, thus belonging to the so-called langasite family. These formerly were studied for their piezoelectricity [18] and their non-linear optical and electro-optical properties [19]. A strong interest in their magnetic behaviour was aroused more recently when it was realized that some of them would materialize kagomé lattice of rare-earth cations [20] or, as in the present case, triangular lattice of triangle units of transition metal cations [21]. As schematized in Fig. 1, this lattice is coplanar to the (a, b) plane and formed in $\text{Ba}_3\text{NbFe}_3\text{Si}_2\text{O}_{14}$ by the Fe^{3+} ions with spin $S=5/2$, which are the only magnetic cations. Consecutive planes are separated by layers containing Ba and Nb cations. The Fe^{3+} ions are tetrahedrally coordinated by oxygens anions, which mediates the superexchange interaction within the triangles. The magnetic interaction between spins belonging to different triangles is mediated by two oxygens (supersuperexchange) in the (a, b) planes and also along the c -axis.

TABLE I: Structural parameters of $\text{Ba}_3\text{NbFe}_3\text{Si}_2\text{O}_{14}$ as refined from X-ray single crystal diffraction data at room temperature. U_{eq} is the isotropic displacement parameter in \AA^2 . The lattice parameters are $a=b=8.539(1)$ \AA , $c=5.2414(1)$ \AA . The agreement factors are : R_{wall} 1.69% and goodness of fit 1.19.%.

Atom	Wyckoff	x	y	z	U_{eq}
Ba	3e	0.56598(2)	0	0	0.00859(4)
Nb	1a	0	0	0	0.00766(6)
Fe	3f	0.24964(4)	0	1/2	0.00776(7)
Si	2d	2/3	1/3	0.5220(1)	0.0063(1)
O(1)	2d	2/3	1/3	0.2162(4)	0.0106(4)
O(2)	6g	0.5259(2)	0.7024(2)	0.3536(3)	0.0118(4)
O(3)	6g	0.7840(2)	0.9002(2)	0.7760(3)	0.0164(4)

It thus is expected to be weaker than the intra-triangle interaction.

Powders of $\text{Ba}_3\text{NbFe}_3\text{Si}_2\text{O}_{14}$ were synthesized by solid state reaction from stoichiometric amounts of Nb_2O_3 , Fe_2O_3 , SiO_2 oxides and BaCO_3 barium carbonate, at 1150 °C in air, within an alumina crucible. The reagents were carefully mixed and pressed to pellets before annealing. The phase purity was checked by X-ray powder diffraction. Single-crystals were grown by the floating-zone method in an image furnace [20]. Small fragments extracted from these were used to investigate the crystal structure on a BrukerNonius kappaCCD x-ray diffractometer using the Ag $K\alpha$ radiation. The anomalous part of the scattering function allowed us to infer the crystal chirality. The one associated with the atomic positions reported in table I is called left-handed, in view of the anti-trigonometric twist of the exchange paths around the c -axis (see Fig. 1 and focus at the J_5 exchange path, which then is the dominant interplane interaction). Note that there are three Fe^{3+} ions per unit cell (labeled in Fig.1) deduced from each other by the 3-fold symmetry.

Magnetization measurements were performed on a $\text{Ba}_3\text{NbFe}_3\text{Si}_2\text{O}_{14}$ single-crystal from 2 to 300 K under magnetic fields up to 10 T on a purpose-built magnetometer. The isotherms of the magnetization M , shown in Fig.2a, are linear and independent on the applied field orientation, parallel (\parallel) or perpendicular (\perp) to the c axis, at least down to the ordering transition temperature. No significant anisotropy is thus detected in the paramagnetic phase as expected for an Fe^{3+} ion with a spin $S=5/2$ and no orbital contribution. At low temperatures, the high field linear part of the magnetization isotherms remains identical for both orientations. The associated susceptibility is shown in Fig. 2b where a cusp at $T_N \approx 27$ K signals the transition towards a magnetic order, also pointed out from a sharp peak in the specific heat [21]. Below T_N , the \parallel magnetization isotherms, as opposed to the \perp ones, exhibit a slight curvature revealing the rise of a small magnetic component along the trigonal c axis. Its value is estimated ≈ 0.014

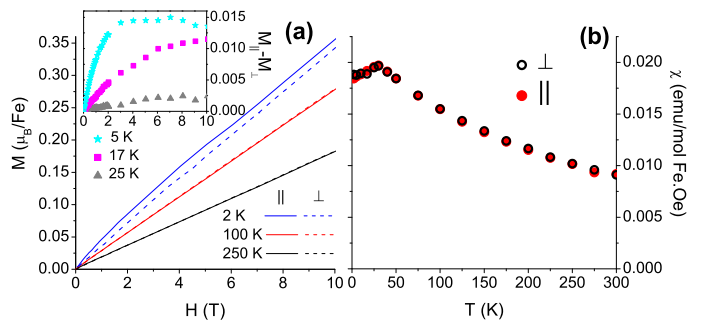


FIG. 2: (Color online) a) Magnetization versus magnetic field with the field applied \parallel or \perp to the c axis. Inset: difference between \parallel and \perp curves below T_N . b) High field susceptibility versus temperature for both \parallel and \perp orientations.

μ_B/Fe at 2 K from the difference between the \perp and \parallel magnetizations (see inset of Fig. 2a). Above 100 K, the magnetic susceptibility is fitted by a Curie-Weiss law $\chi = C/(T - \theta)$, with a Curie constant C corresponding to the effective moment $\mu_{\text{eff}} = g\sqrt{S(S+1)} = 5.92 \mu_B$ of an Fe^{3+} ion and a Curie-Weiss temperature $\theta = -174 \pm 4$ K. The latter indicates predominant antiferromagnetic exchange interactions and suggests magnetic frustration or dimensional reduction since the magnetic ordering occurs at a much lower temperature. A coexistence of phase in a narrow range of temperature around T_N was observed by ^{57}Fe Mössbauer spectroscopy, implying that the magnetic transition would be first order [21].

Neutron diffraction experiments were carried out at the Institut Laue Langevin (ILL), first on powder samples using the D1B diffractometer [21] then on a single crystal using the D15 4-circles diffractometer. Magnetic Bragg peaks emerge below T_N . They can be indexed using the propagation vector $(0, 0, \tau)$ with τ close to $1/7$ [21]. The magnetic structure, as determined from refinement of the powder and single-crystal diffractograms, consists in magnetic moments lying in the (a, b) planes at 120° from each other within each triangle. This magnetic arrangement is accordingly repeated from cell to cell in the (a, b) planes. On moving along the c axis the spins rotate to form a helix of period ≈ 7 lattice parameters. At 2 K, the fitted value of the magnetic moment is $\approx 4 \mu_B$, instead of the expected $5 \mu_B$ for an Fe^{3+} ion. This reduction may result from spin transfer to the oxygen ions [22]. The obtained magnetic structure is consistent with symmetry analysis, which yields three 1-dimensional irreducible representations, leading to the prediction of the two 120° structure with opposite triangular chirality and a structure with ferromagnetic planes helically propagating along the c axis. Whereas powder diffraction is insensitive to the triangular chirality and helicity, single-crystal diffraction can bring additional information on this issue. For clarity in the following and using the trigonometric convention, the term triangular

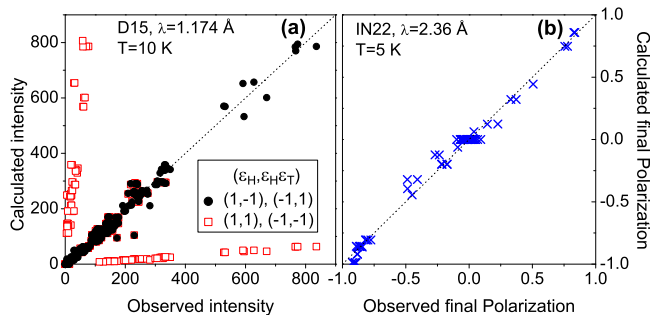


FIG. 3: (Color online) (a) Single crystal diffraction: calculated versus observed integrated magnetic intensities for different $(\epsilon_H, \epsilon_H \epsilon_T)$ pairs (see text). (b) Spherical polarization analysis: calculated versus observed final polarization for 8 magnetic Bragg peaks. The calculated values are those obtained from a refinement of the distribution of domains, which yields the best agreement with the observed values for a single domain of helicity.

chirality will refer to the sense of rotation of the 3 spins within the triangle while going trigonometrically from one corner of the triangle to the others. The term helicity will refer to the sense of rotation of the spins in an helix along the direction of the propagation vector.

The expression of the magnetic moments in the n^{th} unit cell for a perfect helix propagating along the c axis with 3 Bravais lattices (labeled $i=1,2,3$ in Fig.1) is written as $\vec{m}_i(\vec{R}_n) = m \cos(\vec{\tau} \cdot \vec{R}_n + \epsilon_T \Phi_i) \vec{u} + \epsilon_H m \sin(\vec{\tau} \cdot \vec{R}_n + \epsilon_T \Phi_i) \vec{v}$, where \vec{u} and \vec{v} are orthonormal vectors in the (a, b) plane, forming a right handed set with the c axis, and Φ_i is the phase of the i^{th} Bravais lattice. These are accessible from the diffraction data only through the modulus $|\Phi_{i+1} - \Phi_i|$ of their differences. $\epsilon_H = \pm 1$ determines the helicity ($\vec{m}_i(\vec{R}_n) \wedge \vec{m}_i(\vec{R}_n + \vec{c}) = m^2 \sin(\tau) \epsilon_H \vec{c}/|\vec{c}|$) and $\epsilon_H \epsilon_T = \pm 1$ the triangular chirality ($\sum_i \vec{m}_i(\vec{R}_n) \wedge \vec{m}_{i+1}(\vec{R}_n) = (3\sqrt{2}/2)m^2 \epsilon_H \epsilon_T \vec{c}/|\vec{c}|$). Only two pairs among the four possible magnetic chirality states, $(\epsilon_H, \epsilon_H \epsilon_T) = (1,-1)$ and $(-1,1)$, are found compatible with the unpolarized neutron's single-crystal data refined for a left-handed structural chirality (black circles in Fig. 3). An additional experiment on single-crystal using polarized neutrons with spherical polarization analysis was performed using the CRYOPAD device on the IN22 spectrometer at the ILL. This allows one to measure the three orthogonal components of the polarization vector of the neutron beam after scattering by the sample whatever the polarization of the incoming neutron beam. It however suffices to choose three orthogonal orientations of this initial polarisation to get all the accessible informations at a scattering vector (Q_h, Q_k, Q_l) . This leads to nine independent data, giving the components $\bar{P}_{i,j}$ ($i,j=X,Y,Z$ with $X \parallel$ scattering vector and $Z \perp$ scattering plane) of the so-called polarization matrix \bar{P} [23]. This was measured on 8 magnetic peaks of the

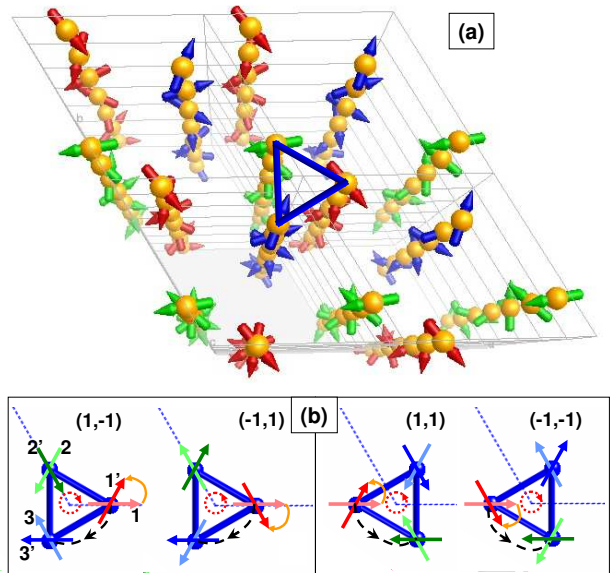


FIG. 4: (Color online) (a) Perspective view of the magnetic structure with different colors for the three Bravais lattices. (b) Representation of the magnetic structures associated to the 4 possible $(\epsilon_H, \epsilon_H \epsilon_T)$ pairs. The light colored moments lie in one layer and the darker colored ones in the next layer along the c axis, an orange curved arrow defines the helicity. The red arrowed circle materializes the triangular chirality. The structural chirality is represented by a diagonal exchange between the two layers (dashed arrow path).

type $(-1, 2, l \pm \tau)$ and $(1, -2, l \pm \tau)$ with $l \in [0,3]$. It is found out from the formalism [24] that the polarization matrices \bar{P} are only sensitive to the helicity ϵ_H , with the components $\bar{P}_{Y,X}$ and $\bar{P}_{Z,X}$ being proportional to the associated distribution of helicity domains. A fit of our data with respect to domain proportions systematically leads to a single helicity in the crystal (see Fig. 3b). This, in turn, indicates the selection of one $(\epsilon_H, \epsilon_H \epsilon_T)$ pair, to agree with the unpolarized diffraction data, thus the selection of the unique associated triangular chirality.

A zero temperature mean-field analysis was undertaken to get more insights about the magnetic structure and to relate it to the crystal structure [25]. A set of five exchange interaction parameters were considered in the Heisenberg Hamiltonian $\mathcal{H} = -\frac{1}{2} \sum_{i,j} J_k \vec{S}_i \cdot \vec{S}_j$, namely J_1 the intra-triangle first neighbor interactions, J_2 the inter-triangle second neighbor interactions in the (a, b) plane and J_3 to J_5 the inter-triangle interactions of adjacent planes (see Fig. 1). These last three supersuperexchange paths are non-equivalent. As from the crystal geometry, it appears that the strongest one (shorter bond lengths and bond angles closer to 180° [26]) would be the diagonal J_5 interaction. It links spins screw-like along the c axis, trigonometrically (anti-trigonometrically) for right-handed (left-handed) structural chirality. With an-

tiferromagnetic J_1 and J_2 and null inter-plane interactions (J_3 to $J_5=0$), the diagonalization of the Fourier transform of the interaction matrix yields three solutions with zero propagation vector : a less favored ferromagnetic order and two degenerate 120° spin structures with opposite triangular chirality. With additional weak inter-plane interactions where one diagonal interaction prevails over the other two, a helical modulation is generated along the c axis and the degeneracy of the two 120° spin configurations is lifted. The favored solution for left-handed structural chirality then corresponds to the two $(\epsilon_H, \epsilon_H\epsilon_T)$ pairs found with unpolarized neutrons single-crystal diffraction. Inverting the structural chirality we get the two other $(\epsilon_H, \epsilon_H\epsilon_T)$ pairs (see Fig.4b).

Additional understanding can be gained by simple geometrical considerations. Given the 120° spin structure in the triangles, if one considers only one predominant diagonal antiferromagnetic interaction between adjacent layers, one atom of a given triangle will be anti-aligned with the atom of the upper triangle in the diagonal direction (*e.g.* atoms 1 and 3' in Fig. 4b). This will result in a rotation by 60° of the spins along the c axis (*e.g.* from atom 1 to atom 1') leading to a propagation vector $(0, 0, 1/6)$, close to the value determined in $\text{Ba}_3\text{NbFe}_3\text{Si}_2\text{O}_{14}$. The departure from $1/6$ can be ascribed to the contribution of the other two inter-plane interactions. Therefore, the observed magnetic arrangement is well described by the 5 considered exchange interactions. This is unlike MnSi or CsCuCl₃, where the helices are generated from Dzyaloshinskii-Moriya interactions [5, 7]. The mean field calculation though can only access the modulus of the phase difference and is energetically favorable to two $(\epsilon_H, \epsilon_H\epsilon_T)$ solutions. As polarized neutrons have shown that one of this solution only is actually observed, the origin of this ultimate selection is still unclear. It could be due to the Dzyaloshinskii-Moriya antisymmetric interaction, allowed in this compound. Another hint for the presence of this interaction is the small ferromagnetic component observed along the c axis in the magnetization isotherms (see Fig. 2a).

It is clear from our results that $\text{Ba}_3\text{NbFe}_3\text{Si}_2\text{O}_{14}$ could raise a strong interest in the field of multiferroism. Indeed, although unexpected when the propagation vector is perpendicular to the helix plane [27, 28], the onset of an electrical polarisation was observed at the magnetic ordering temperature in another trigonal helically stacked triangular antiferromagnets with a 120° spin structure [14]. Two chiral magnetic domains coexist in this centrosymmetric compound. From phenomenological symmetry arguments, the amplitude of the electrical polarization was related to the unbalance between these two domains. If this argument holds, the effect should be maximum in $\text{Ba}_3\text{NbFe}_3\text{Si}_2\text{O}_{14}$ since the chirality is single domain. To probe this, measurements of the dielectric constant were performed. An anomaly was observed at the onset of the magnetic order. This will be completed with electric

polarisation measurements and reported elsewhere.

In conclusion, the Fe-langasite $\text{Ba}_3\text{NbFe}_3\text{Si}_2\text{O}_{14}$ provides the first evidence of a totally chiral state from the structural point of view where it manifests itself by the twist of the exchange paths and from the magnetic point of view where two different kinds of chiralities, within the triangles and along the helices, coexist and interplay.

This work was financially supported by the ANR 06-BLAN-01871. We would like to thank B. Canals and L.-P. Regnault for fruitful discussions and for the help during the polarized neutron experiment for the latter.

-
- [1] H. D. Flack, *Helvetica Chimica Acta* **86**, 905 (2003).
 - [2] J. Villain, *J. Phys. and Chem. Solids* **11**, 303 (1959).
 - [3] A. Yoshimori, *J. Phys. Soc. Jap.* **14**, 807 (1959).
 - [4] I. E. Dzyaloshinskii, *Soviet Physics JETP* **19**, 960 (1964).
 - [5] P. Bak and M. H. Jensen, *J. Phys. C* **13**, L881 (1980).
 - [6] O. Nakanishi, A. Yanase, A. Hasegawa, *et. al.*, *Solid St. Comm.* **35**, 995 (1980).
 - [7] K. Adachi, N. Achiwa, and M. Mekata, *J. Phys. Soc. Jap.* **49**, 545 (1980).
 - [8] K. Siratori, J. Akimitsu, E. Kita, *et. al.*, *J. Phys. Soc. Jap.* **48**, 1111 (1980).
 - [9] V. P. Plakhity, J. Wosnitza, J. Kulda, *et. al.*, *Physica B* **385**, 288 (2006).
 - [10] S. V. Maleyev, *Physica B* **397**, 11 (2007).
 - [11] A. Gukasov, *Physica B* **267**, 97 (1999).
 - [12] G. Shirane, R. Cowley, C. Majkrzak, *et. al.*, *Phys. Rev. B* **28**, 6251 (1983).
 - [13] D. Grohol, K. Matan, J.-H. Cho, *et. al.*, *Nature Materials* **4**, 323 (2005).
 - [14] M. Kenzelmann, G. Lawes and A. B. Harris, *et. al.*, *Phys. Rev. Lett.* **98**, 267205 (2007).
 - [15] H. Kawamura and S. Miyashita, *J. Phys. Soc. Jap.* **53**, 9 (1984).
 - [16] M. Elhajal, B. Canals, C. Lacroix, *Phys. Rev. B* **66**, 014422 (2002); R. Ballou, B. Canals, M. Elhajal, *et. al.*, *J. Magn. Magn. Mat.* **262**, 465 (2003).
 - [17] J. T. Chalker, P. C. Holdsworth, and E. F. Shender, *Phys. Rev. Lett.* **68**, 855 (1992).
 - [18] T. Iwataki, H. Ohsato, K. Tanaka, *et. al.*, *J. Eur. Ceram. Soc.* **21**, 1409 (2001).
 - [19] Y. Xin, W. Jiyang, Z. Huaijin, *et. al.*, *Jap. J. Appl. Phys* **41**, 7419 (2002).
 - [20] P. Bordet, I. Gelard, K. Marty, *et. al.*, *J. Phys.: Condens. Matter* **18**, 5147 (2006).
 - [21] K. Marty, V. Simonet, P. Bordet, *et. al.*, to be published in *J. Magn. Magn. Mat.* (2008).
 - [22] V. C. Rackhecha, and N. S. Sayta Murthy, *J. Phys. C.:Solid State Phys.* **11**, 4389 (1978).
 - [23] F. Tasset, P. J. Brown, E. Lelièvre-Berna, *et. al.*, *Physica B* **267**, 69 (1999).
 - [24] M. Blume, *Phys. Rev.* **130**, 1670 (1963).
 - [25] E. F. Bertaut, *J. Phys. Chem. Solids* **21**, 256 (1961).
 - [26] J. B. Goodenough, *Phys. Rev.* **100**, 564 (1955). J. Kanamori, *J. Phys. Chem. Solids* **10**, 87 (1959).
 - [27] M. Mostovoy, *Phys. Rev. Lett.* **96**, 067601 (2006); S.-W. Cheong, M. Mostovoy, *Nature* **6**, 13 (2007).
 - [28] H. Katsura, N. Nagaosa, A. V. Balatsky, *Phys. Rev. Lett.*

95, 057205 (2005).